Fractal ladder models and power law wave equations

James F. Kelly[a)]
Department of Applied Mathematics, Naval Postgraduate School, Monterey, California 93943

Robert J. McGough
Department of Electrical and Computer Engineering, Michigan State University, East Lansing, Michigan 48824

(Received 9 December 2008; revised 20 July 2009; accepted 21 July 2009)

The ultrasonic attenuation coefficient in mammalian tissue is approximated by a frequency-dependent power law for frequencies less than 100 MHz. To describe this power law behavior in soft tissue, a hierarchical fractal network model is proposed. The viscoelastic and self-similar properties of tissue are captured by a constitutive equation based on a lumped parameter infinite-ladder topology involving alternating springs and dashpots. In the low-frequency limit, this ladder network yields a stress-strain constitutive equation with a time-fractional derivative. By combining this constitutive equation with linearized conservation principles and an adiabatic equation of state, a fractional partial differential equation that describes power law attenuation is derived. The resulting attenuation coefficient is a power law with exponent ranging between 1 and 2, while the phase velocity is in agreement with the Kramers–Kronig relations. The fractal ladder model is compared to published attenuation coefficient data, thus providing equivalent lumped parameters. © *2009 Acoustical Society of America.* [DOI: 10.1121/1.3204304]

PACS number(s): 43.80.Cs, 43.20.Hq, 43.35.Bf [TDM] Pages: 2072–2081

I. INTRODUCTION

The attenuation coefficient in human and mammalian tissue in the ultrasonic range has a power law dependence on frequency.[1–3] The power law exponent typically ranges between 1 and 1.7 for most tissue.[2,4] Moreover, the power law exponent has been experimentally correlated with the pathological state of tissue.[2,5,6] Classical theories for ultrasonic absorption, such as thermo-viscosity,[7] and Biot's porous media theories[8] predict a frequency-squared dependence in the low-frequency limit, while classical relaxation predicts an attenuation coefficient with a resonant peak at the relaxation frequency of the material. However, neither of these behaviors is observed in soft tissue. Multiple-relaxation mechanism models[9] predict power law behavior over a narrow frequency band by empirically choosing the proper weights and relaxation frequencies, yet these models also fail to explain power law behavior over large frequency bands.

Other phenomenological models for ultrasonic attenuation in biological media have also been proposed. Frequency-domain descriptions include the linear phase model,[10] the Hilbert dispersive model,[11] the material impulse response model,[12] and power law models.[13–15] These methods evaluate a frequency-dependent transfer function and then perform a numerical inverse Fourier transform. Attenuation and dispersion have also been modeled directly in the time-domain via partial differential equations (PDEs) and fractional partial differential equations (FPDEs). PDE formulations incorporate loss via integer-ordered derivatives,[16,17] whereas FPDEs add loss to the wave equation with a time-fractional derivative,[18,19] a space-fractional derivative,[20,21] or the combination of an integer-ordered spatial derivative and a time-fractional derivative.[22,23] Nonlinear dissipative propagation has also been described with fractional spatial derivatives via generalizations of Burgers equation,[24] as well as transient elastic wave propagation in porous[25] and viscoelastic media.[26] These FPDE models build on previous applications of fractional calculus to diffusion processes,[27,28] relaxation processes,[29] viscoelasticity,[30,31] and seismology.[22] A third approach utilizes doublet mechanics,[32] whereby discrete microstructures are incorporated into the wave equation.

Within the viscoelastic and biomechanics communities, lumped parameter networks, such as the Maxwell and Voigt models, are commonly employed[33,34] to model the mechanical response of cells[34–36] and bulk tissue[37,38] to an applied force. Lumped parameter networks have also been extended to include infinite-ladder networks consisting of alternating elastic and viscous elements[33,39–41] and fractal tree networks,[42] which generate time-fractional rheological constitutive equations[30] for polymers. As discussed in Refs. 39, 33, and 40–42, the time-fractional derivative in the constitutive equation captures the (1) elastic, (2) viscous, and (3) self-similar properties described by these infinite networks. To date, however, fractal ladder networks have not been applied to dispersion in soft tissue. Moreover, time-fractional derivatives have been linked with diffusion[27] and relaxation[28] on fractal structures. In these studies, the order of the fractional derivative is a function of the fractal dimension of the underlying geometry. Within the ultrasonics community, however, this quantitative relationship between the fractal nature of tissue and FPDE has not been explored quantitatively.

This paper describes a model for the dissipative properties of soft tissue that employs hierarchical fractal networks.

[a)]Author to whom correspondence should be addressed. Electronic mail: jfkelly@nps.edu

Section II provides biological motivation and a review of linear stress-strain relationships in viscoelastic materials. A ladder model is then proposed by considering fractal networks of springs and dashpots.[33,40–42] Section III derives a fractional constitutive equation from the ladder model using tools from fractional calculus. On the basis of this constitutive equation, a FPDE utilizing a combination of integer-ordered spatial derivatives and a time-fractional derivative is derived from basic conservation laws in Sec. IV for linear macro-homogeneous media. This FPDE, which was originally proposed within the seismology community[22] and later considered in the biomedical acoustics community,[23] yields both a power law attenuation coefficient and a phase velocity predicted by the Kramers–Kronig relationships. In Sec. V, the ladder model is matched to published data and analyzed in terms of previous biomechanical and fractal models, followed by the conclusion in Sec. VI.

II. FRACTAL LADDER MODEL

This section introduces a lumped parameter, fractal ladder network to model the stress-strain relationship in biological media. From this fractal ladder network, a time-fractional derivative constitutive equation is derived, thus providing a physical basis for time-fractional FPDE such as the models proposed by Caputo[22] for seismic wave propagation in the earth and Wismer[23] for ultrasonic wave propagation in tissue.

A linear constitutive equation postulates a functional relationship between the time-dependent stress tensor $T_{ij}(t)$ and time-dependent strain tensor $\epsilon_{ij}(t)$ via a differential, integral, or integro-differential relationship that satisfies the principle of superposition. Familiar examples of constitutive equations, such as Hooke's law for an elastic solid and Newton's law for a viscous fluid, fail to predict the behavior of many viscoelastic solids; therefore, generalized viscoelastic models involving fractional derivatives and integrals have been developed.[30,31] This section proposes a constitutive equation for biological media using a fractal ladder network as a lumped parameter model. A qualitative biological model is first postulated, followed by the basic theory of viscoelasticity for a linear, non-Newtonian fluid.

A. Biological motivation

A mechanical model for the loss mechanism in mammalian biological tissue is motivated in this section. This model satisfies a power law attenuation coefficient $\alpha(\omega)$ of the form

$$\alpha(\omega) = \alpha_0|\omega|^y \tag{1}$$

over an appropriate frequency band, where ω is angular frequency and $1 < y \leq 2$ is the power law exponent. Soft tissue consists of hierarchical arrangements of elastic and fluid-like components. These tissues are highly heterogeneous and composed of over a hundred distinct cell types.[43] Each tissue consists of aggregates of cells suspended by a fluid-like extra-cellular matrix (ECM). The ECM is often modeled as an aqueous solution of viscoelastic polymers, which possess both solid and fluid-like properties. Individual cells are modeled as elastic membranes containing fluid-like cytoplasm.[34] Within the cytoplasm are distributed organelles, such as the nucleus, endoplasmic reticulum, and lysosomes, which in turn have an elastic membrane containing with a fluid-like interior.[43]

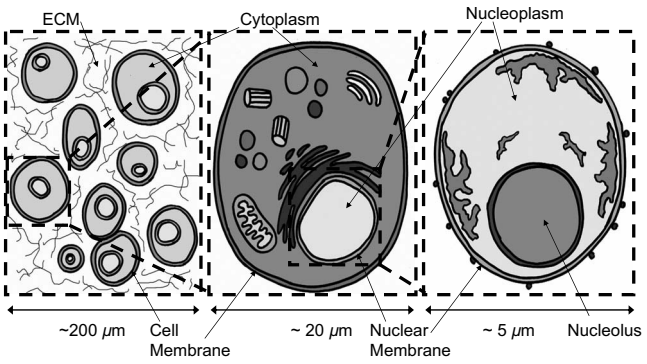

FIG. 1. Schematic showing tissue structure at three different spatial scales (tissue, cellular, and sub-cellular). The first panel ($\sim$200 μm) displays an ensemble of mammalian cells, each bounded by an elastic membrane, suspended in a viscoelastic ECM. The second panel ($\sim$20 μm) displays an individual cell at a higher level of magnification. The third panel ($\sim$5 μm) displays the cell nucleus, consisting of a double membrane, a fluid-like nucleoplasm, and an elastic nucleolus in the interior, which contains chromatin (Ref. 43). Although the specific biological structures vary at each successive spatial scale, the essential features are the same: fluid substrates containing elastic compartments. This self-similar pattern forms the basis for the fractal structure shown in Fig. 2.

This hierarchical arrangement is displayed at several scales in Fig. 1. Panel (a), which is on the scale of 200 μm, contains an ensemble of mammalian cells, each bounded by an elastic membrane that is suspended in a viscoelastic ECM. Both the ECM and cytoplasm consist of complex polymers (e.g., collagen) dissolved in a viscous fluid. The resulting structure is therefore a viscoelastic material. In panel (b), which is on the scale of 20 μm, an individual cell is shown at a higher level of magnification. Inside the elastic membrane is the cytoplasm, which has viscoelastic properties that are similar to the ECM. Panel (c) displays the cell nucleus on the scale of 5 μm, consisting of a double membrane, a fluid-like nucleoplasm, and an elastic nucleolus in the interior, which contains chromatin.[43] Based on the structure shown in Fig. 1, both the viscoelastic properties and self-similar, or fractal, properties of tissue are evident, which motivates a simplifying hierarchical mathematical model. Applying this biological picture, tissue may be visualized as a recursive arrangement of fluid substrates containing elastic membranes. Similar models, known as liquid drop models, have been proposed within the biomechanics community to describe the deformation of eukaryotic cells.[34,35] These liquid drop models typically model the cell membrane as a cortical layer with a characteristic surface tension, whereas the cytoplasm in the cell interior is modeled as a viscous, incompressible fluid with a characteristic coefficient of viscosity. The cell nucleus may also be included as an additional elastic component embedded within the viscous fluid.

In the following fractal model for the viscoelastic properties of tissue, an infinite number of nested elastic membranes, each containing a viscous compressible fluid, is proposed. By defining an infinite number of layers, larger structures (e.g., ensembles of cells) and smaller structures (e.g., cell nuclei) may be included within the lumped param-

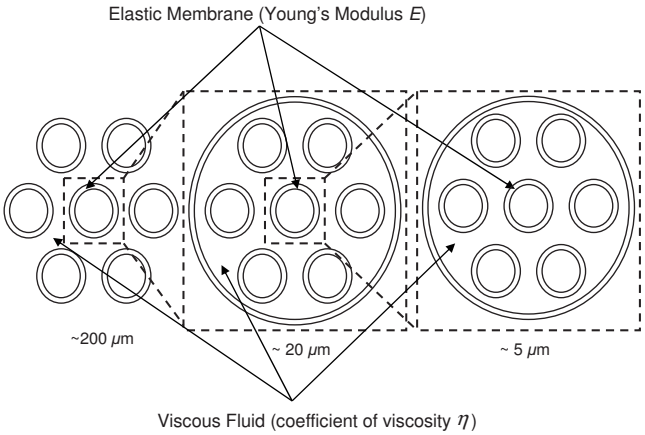

FIG. 2. Layered fractal model for biological tissue based on the schematic shown in Fig. 1. The first panel displays an infinite number of thin elastic membranes with Young's modulus E alternating with viscous compartments that have coefficients of viscosity η. The second panel zooms in on the first panel, thus showing the self-similar layered structure.

eter framework. By allowing the number of structural components to extend indefinitely, the self-similarity of biological media is revealed. This topology is depicted in Fig. 2, where the alternating elastic and viscous components are visualized as a self-similar hexagonal packing of spheres within spheres. Each of the three panels in Fig. 2 corresponds to the three panels in Fig. 1. That is, the left panel of Fig. 2 models the tissue level, the center panel models the cellular level, and the right panel models the sub-cellular level. Comparing the three panels of Figs. 1 and 2, the self-similar nature of this fractal structure is immediately evident. Hence, this fractal model captures the three essential features of the biological picture shown in Fig. 1: (1) elastic membranes, (2) fluid compartments, and (3) self-similarity over a range of spatial scales.

In order to capture these three salient properties of biological media, a fractal network of springs and dashpots is proposed in Fig. 3. The elastic membranes displayed in Fig. 2 are represented by springs with Young's modulus E, while the viscous compartments are represented by dashpots with coefficients of viscosity η. Each level in Fig. 3 corresponds

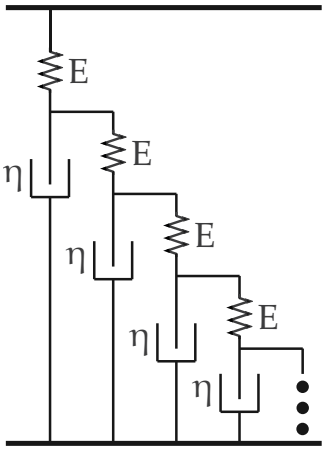

FIG. 3. Fractal ladder model for tissue micro-structure. The continuum model depicted in Fig. 2 is described by an infinite fractal ladder consisting of springs with Young's modulus E and coefficients of viscosity η.

to a pair of elastic/viscous layers shown in Fig. 2 and an individual level of magnification in Fig. 1. This fractal network is analyzed in depth in Sec. II C. Similar fractal networks have previously been used in lumped parameter models of viscoelastic systems[39,44] such as cross-linked polymers and gels.[41]

B. Stress-strain relationships

In this section, the well-known constitutive equation for a viscous Newtonian fluid relating the strain ϵ_{ij} and stress T_{ij} tensors is generalized to self-similar biological media. The strain tensor is defined via $\epsilon_{ij}=\partial w_i/\partial x_j$, where w_i denotes the ith component of displacement. The stress tensor T_{ij} denotes the ith component of stress per unit area along a surface normal to the jth direction, where $1\leq i, j\leq 3$ denote the x, y, and z directions. The viscous stress tensor T_{ij} for a compressible, viscous fluid with pressure p and velocity $\mathbf{u}$ is given by[7]

$$T_{ij}=-p\delta_{ij}-\frac{2}{3}\mu\nabla\cdot\mathbf{u}\delta_{ij}+\mu\left(\frac{\partial u_i}{\partial x_j}+\frac{\partial u_j}{\partial x_i}\right), \tag{2}$$

where μ is the coefficient of shear viscosity, δ_{ij} is the Kronecker delta operator, and $i,j=1, 2, 3$. For homogeneous gases, μ may be computed via kinetic theory. For more complicated fluids, μ must be measured experimentally. Equation (2) contains three terms: (1) an elastic term involving the thermodynamic pressure p, (2) an isotropic frictional term, and (3) a shearing term. In Eq. (2), the coefficient of bulk viscosity is assumed to be zero.

Although Eq. (2) may describe the stress-strain relationship on a sufficiently small micro-scale with a variable viscosity μ, Eq. (2) fails to predict dissipative behavior on the macro-scale in most biological media. To obtain a constitutive equation on a scale commensurate with an acoustic wavelength (macro-scale), Eq. (2) is averaged over a sufficiently large volume to achieve a constitutive equation with a constant coefficient. This averaging, or up-scaling procedure, should account for the signature micro-heterogeneity and hierarchical micro-structure of biological media. One simple up-scaling procedure employs the lumped parameter model discussed in Sec. II A, wherein the individual components of the medium (cells, membranes, organelles, etc.) are represented via hierarchical arrangements of springs and dashpots.

On the macro-scale, the normal stress is decomposed according to

$$T_{ij}(\mathbf{r},t)=-p(\mathbf{r},t)\delta_{ij}+\sigma_{ij}(\mathbf{r},t), \tag{3}$$

where $\sigma(\mathbf{r},t)$ is the component of stress responsible for dissipation. For a viscous medium, $\sigma(\mathbf{r},t)$ corresponds to the second and third terms in Eq. (2). For a linear material, $\sigma_{ij}(\mathbf{r},t)$ is a linear function of strain $\epsilon_{ij}(\mathbf{r},t)$. The dissipative component of Eq. (2) can be generalized to include memory effects by relating each component of stress and strain to a causal, stationary, hereditary integral (or Boltzmann superposition integral):[33]

$$\sigma_{ij}(\mathbf{r},t) = \int_{-\infty}^{t} g(t-t')\left[-\frac{2}{3}\sum_{t=1}^{3}\epsilon_{il}(\mathbf{r},t')\delta_{ij} + \epsilon_{ij}(\mathbf{r},t') + \epsilon_{ji}(\mathbf{r},t')\right]dt', \tag{4}$$

where $g(t)$ is a *relaxance*, or memory, function[33] which relates the present state of the material to the previous history. Since Eq. (4) is a convolution integral, the stress-strain relationship becomes multiplication in the Laplace domain. In one dimensional (1D), the stress tensor has only the component $\epsilon(t)=\epsilon_{11}(t)$, yielding the convolution $\sigma=4/3g(t)*\epsilon(t)$. Applying a Laplace transform and invoking the convolution theorem yields

$$\hat{\sigma}(\mathbf{r},s) = \tfrac{4}{3}\hat{g}(s)\hat{\epsilon}(\mathbf{r},s). \tag{5}$$

C. Infinite ladder

In this section, a fractal ladder model is constructed in 1D. By assuming that tissue is isotropic on the macro-scale, the 1D model is then extended to three dimensional (3D). The combined viscous and elastic components are modeled as springs and dashpots, respectively. Springs, which model energy storage, represent the nested elastic membranes shown in Fig. 2, while dashpots, which model dissipation, represent the viscous components, such as cytoplasm. The self-similar structure is realized as a fractal ladder in Fig. 3, which provides a lumped parameter description of the geometric model shown in Fig. 2. All of the springs in this model have the same spring constant, or Young's modulus, E and all of the dashpots have the same coefficient of viscosity η. The transfer function $\hat{g}(s)$ for the stress-strain relationship given by Eq. (5) is then evaluated as an infinite, periodic continued fraction:

$$\hat{g}(s) = \eta s + \cfrac{1}{E^{-1} + \cfrac{1}{\eta s + \cfrac{1}{E^{-1} + \cdots}}} = \frac{-\eta s/E + \sqrt{\eta s/E(\eta s/E + 4)}}{2/E}, \tag{6}$$

where the periodic continued fraction is evaluated in closed form.[41,42] For $s\eta/E \ll 1$, the binomial approximation is applied, yielding the low-frequency approximation

$$\hat{g} \approx \sqrt{\eta E s}. \tag{7}$$

Inserting Eq. (7) into Eq. (5), and performing an inverse Laplace transform by applying Eq. (A2) from Appendix A, yields

$$\sigma = \frac{4}{3}\sqrt{\eta E}\frac{\partial^{1/2}\epsilon}{\partial t^{1/2}}, \tag{8}$$

where the fractional derivative operator is defined by Eq. (A1) in Appendix A.

The ladder model can also be considered as a fundamental mechanical component (a "springpot"[45]), allowing more complicated fractal networks, or recursive ladders, to be constructed. For instance, consider a recursive ladder model constructed by replacing the viscous damper in Fig. 3 with a fractal ladder, producing the arrangement shown in Fig. 4. Similarly, a recursive ladder may be constructed by replacing the springs in Fig. 3 with a fractal ladder, producing the arrangement shown in Fig. 5. As shown in Appendix B, the ladder model may be generalized to recursive ladder topologies. Similar fractal tree networks were considered in Ref. 42 to model the power law response of polymers. These recursive ladder models, which are developed in Appendix B, yield the stress-strain relationship

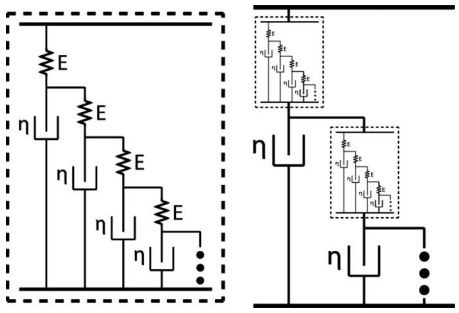

FIG. 4. Example of a recursive fractal ladder model where the dampers in the simple ladder shown in Fig. 3 are replaced with ladders. This particular fractal arrangement is denoted by $(M,N)=(0,1)$ and yields a fractional derivative with $\beta=1/4$.

$$\sigma = \frac{4}{3}\eta^{\beta}E^{1-\beta}\frac{\partial^{\beta}\epsilon}{\partial t^{\beta}}, \tag{9}$$

which is a generalization of Eq. (8) for all $0<\beta\leq 1$. The fractional derivative order β is specified by (see Appendix B)

$$\beta = \frac{1}{2}\left(1 - \frac{1}{2^M} + \frac{1}{2^N}\right), \tag{10}$$

where M is the depth of recursion of the dampers and N is the depth of recursion of the springs. In the special case of the simple ladder $(M,N)=(0,0)$, the recursive ladder reduces to the simple ladder with $\beta=1/2$. For $M\neq N$, different fractional orders β are obtained. For instance, if $(M,N)=(1,0)$, then each damper in Fig. 3 is replaced by a ladder, yielding $\beta=3/4$. If $(M,N)=(0,1)$, then each spring in Fig. 3 is replaced by a ladder, yielding $\beta=1/4$. Note that Eq. (10) does not uniquely define β for given $M,N\geq 0$. For instance, the

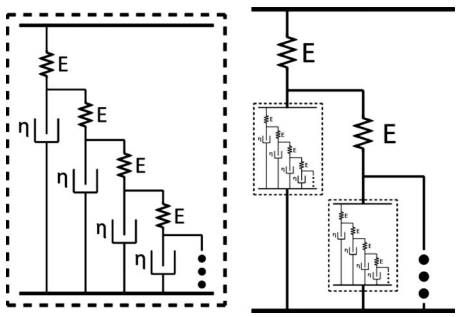

FIG. 5. Example of a recursive fractal ladder model where the springs in the simple ladder shown in Fig. 3 are replaced with ladders. This particular fractal arrangement is denoted by $(M,N)=(1,0)$ and yields a fractional derivative with $\beta=3/4$.

value of $\beta=1/2$ is recovered for any choice of $M=N$.

III. 3D FRACTIONAL CONSTITUTIVE EQUATION AND WAVE EQUATION

A. Fractional constitutive equation

Generalizing Eq. (9) to 3D (under the macro-isotropic assumption) yields

$$\sigma_{ij} = -\left(\frac{2}{3}E_0^{1-\beta}\eta_0^{\beta}\frac{\partial^{\beta}}{\partial t^{\beta}}\sum_{j=1}^{3}\epsilon_{ij}\right)\delta_{ij} + E_0^{1-\beta}\eta_0^{\beta}\frac{\partial^{\beta}}{\partial t^{\beta}}(\epsilon_{ij}+\epsilon_{ji}). \tag{11}$$

Constitutive equations similar to Eq. (14) have been previously proposed for viscoelastic materials within the geology community.[22] Similar to Eq. (2), Eq. (11) is expressed in terms of the particle velocity $\mathbf{u}$, yielding

$$\sigma_{ij} = -\left(\frac{2}{3}E_0^{1-\beta}\eta_0^{\beta}\frac{\partial^{\beta}}{\partial t^{\beta}}\sum_{j=1}^{3}\epsilon_{ij}\right)\delta_{ij} + E_0^{1-\beta}\eta_0^{\beta}\frac{\partial^{\beta-1}}{\partial t^{\beta-1}}\left(\frac{\partial u_i}{\partial x_j} + \frac{\partial u_j}{\partial x_i}\right), \tag{12}$$

where Einstein summation notation is utilized. Thus, a time-fractional stress-strain relationship follows from the fractal ladder originally proposed for polymer modeling in Ref. 41. Equation (12) consists of two viscoelastic terms involving the fractional derivative of strain with respect to time, where the fractional derivative term is responsible for the coupled processes of attenuation and dispersion. For $\beta<1$, Eq. (12) displays a temporal non-locality commonly utilized in phenomenological viscoelasticity.[22,30] Theoretical justification for constitutive equations similar to Eq. (12) was also established[31] on the basis of dilute solutions of polymers[46] within a homogeneous, Newtonian solvent.

By identifying a generalized coefficient of viscosity

$$\mu = E_0^{1-\beta}\eta_0^{\beta}, \tag{13}$$

the following averaged constitutive equation involving velocity gradients is computed:

$$T_{ij} = -p\,\delta_{ij} - \frac{2}{3}\mu\frac{\partial^{\beta-1}}{\partial t^{\beta-1}}\frac{\partial u_i}{\partial x_i}\delta_{ij} + \mu\frac{\partial^{\beta-1}}{\partial t^{\beta-1}}\left(\frac{\partial u_i}{\partial x_j}+\frac{\partial u_j}{\partial x_i}\right). \tag{14}$$

For $\beta=1$, Eq. (14) reduces to the viscous stress tensor for a compressible, Newtonian fluid given by Eq. (2). Equation (14) contains three terms: (1) an elastic term involving the thermodynamic pressure p, (2) an isotropic frictional term, and (3) a shearing term. The frictional terms tend to diffuse momentum through the flow. In a viscous fluid ($\beta=1$), the frictional term involves only an integer-ordered derivative and is purely local. For a homogeneous fluid with simple molecular structure, this relation properly accounts for momentum diffusion. For biological tissue, however, viscous loss does not properly account for observed dissipation. Tissue is both heterogeneous and has a complex molecular structure that can be modeled as a viscoelastic medium. Physically, momentum may diffuse faster and/or slower in some directions due to the heterogeneity of tissue. To describe these effects, the local constitutive relationship is generalized by a global relation that incorporates memory into the flow. The temporal operator $\partial^{\beta-1}/\partial t^{\beta-1}$ is the Riemann–Liouville fractional derivative for $0<\beta<1$. Thus, the viscous shearing term in a standard Newtonian fluid is replaced with a memory term which relates the stress at time t to the entire history of the velocity gradient. Similar hereditary constitutive equations, which utilize time-fractional and time-convolutional operators, are widely used in theoretical viscoelasticity.[26,47]

B. 3D fractional wave equation

A time-fractional wave equation was originally introduced by Caputo[22] to model dissipative elastic wave motion in geological media. Equation (8) in Ref. 22 contains a FPDE that models 1D, plane wave propagation in a viscoelastic solid. Later, Wismer[23] independently obtained a 3D version of this equation that models ultrasonic wave motion in power law biological media. This section demonstrates how the fractal ladder model and fractional constitutive equation in Sec. II lead to a FPDE that describes dispersive wave propagation in biological media. In particular, the 3D fractional wave equation,[23] which models power law attenuation via a time-fractional derivative, is derived for a linear, macro-homogeneous, and isotropic medium governed by Eq. (14). Since this derivation is similar to the derivation of the thermoviscous wave equation presented in Ref. 7, only the major points are emphasized here.

Linear, longitudinal wave motion is considered in a homogeneous medium with density ρ_0, sound speed c_0, and generalized viscosity μ. Here, shear mode propagation is neglected. The adiabatic hypothesis, whereby entropy is assumed constant, is also adopted; thus the additional dissipative effects of thermal conduction are neglected. Equation (14) is complemented by (1) the linearized Cauchy's equation, (2) the linearized, adiabatic equation of state, and (3) the linearized equation of continuity. The linearized Cauchy equation, which neglects the convective term $\mathbf{u}\cdot\nabla\mathbf{u}$, restates Newton's second law of motion as

$$\rho_0\frac{\partial u_i}{\partial t} = \frac{\partial T_{ij}}{\partial x_j}. \tag{15}$$

The linearized, adiabatic equation of state is given by $p=c_0^2\delta\rho$, where $\delta\rho$ denotes excess density and c_0 is the adiabatic speed of sound. Finally, the linearized equation of continuity is given by

$$\frac{\partial\delta\rho}{\partial t} + \rho_0\frac{\partial u_i}{\partial x_i} = 0, \tag{16}$$

which accounts for local mass conservation. First, the divergence of Eq. (14) is evaluated and inserted into Eq. (15). Neglecting the transverse component of velocity (see Ref. 7 for details) yields

$$\rho_0\frac{\partial u_i}{\partial t} = -\frac{\partial p}{\partial x_i} + \frac{4}{3}\mu\nabla^2 u_i. \tag{17}$$

Applying the divergence operator to both sides of Eq. (17) yields

$$\rho_0 \frac{\partial}{\partial t}\left(\frac{\partial u_i}{\partial x_i}\right) = -\nabla^2 p + \frac{4}{3}\mu \frac{\partial^{\beta-1}}{\partial t^{\beta-1}}\nabla^2\left(\frac{\partial u_i}{\partial x_i}\right). \tag{18}$$

Finally, to derive a wave equation in terms of the pressure, Eq. (16) is combined with the equation of state and inserted into Eq. (18), yielding

$$\frac{1}{c_0^2}\frac{\partial^2 p}{\partial t^2} = \nabla^2 p + \frac{4\mu}{3c_0^2\rho_0}\frac{\partial^\beta}{\partial t^\beta}\nabla^2 p. \tag{19}$$

Identifying the relaxation time

$$\tau^\beta = \frac{4\mu}{3c_0^2\rho_0} \tag{20}$$

yields the 3D fractional wave equation[23]

$$\nabla^2 p - \frac{1}{c_0^2}\frac{\partial^2 p}{\partial t^2} + \tau^{y-1}\frac{\partial^{y-1}}{\partial t^{y-1}}\nabla^2 p = 0, \tag{21}$$

where $y=\beta+1$ is the power law exponent. Frequency-dependent loss is incorporated via the Riemann–Liouville fractional derivative defined in Appendix A. Equation (21) is identical to Eq. (5) in Ref. 23 and may be expressed as Eq. (8) in Ref. 22 for 1D problems. For $y=2$, Eq. (21) reduces to the Stokes wave equation,[48], which models wave propagation in a homogeneous, viscous medium. As shown in Ref. 23, for $y>1$, Eq. (21) admits an attenuation coefficient with a power law dependence in the low-frequency limit. For $y=1$, however, the loss operator reduces to a spatial Laplacian, and this equation thereby fails to model power law attenuation. For this reason, the exponent is restricted to $1<y\leqslant 2$. Hence, Eq. (21) arises naturally as a wave equation that models small-amplitude, longitudinal disturbances in media governed by the fractional constitutive equation given by Eq. (14). In addition, the parameter τ appearing in Eq. (21) is given physical meaning by Eq. (20), which depends on the micro-structural properties of the medium μ as well as the macroscopic properties c_0 and ρ_0.

C. Power law attenuation

Several important relations, which were discussed in Refs. 22 and 23, are briefly reviewed in this subsection. To derive a power law attenuation coefficient for Eq. (21), the dispersion relationship between angular frequency ω and spatial wavenumber k is calculated. Applying a space-time Fourier transform to Eq. (21) yields

$$-k^2 + \frac{\omega^2}{c_0^2} - k^2\tau^{y-1}(j\omega)^{y-1} = 0. \tag{22}$$

Solving for the wavenumber $k(\omega)$ yields

$$k(\omega) = \frac{\omega}{c_0\sqrt{1+(j\tau\omega)^{y-1}}}. \tag{23}$$

In the low-frequency limit, the binomial approximation is applied, yielding

$$k(\omega) \approx \frac{\omega}{c_0}\left(1 - \frac{\tau^{y-1}}{2}\cos\left(\frac{(y-1)\pi}{2}\right)\omega^{y-1} - j\frac{\tau^{y-1}}{2}\sin\left(\frac{(y-1)\pi}{2}\right)\omega^{y-1}\right) \tag{24}$$

for an outgoing wave. The attenuation coefficient $\alpha(\omega)$ is computed by taking the imaginary part of Eq. (24), yielding the power law coefficient given by Eq. (1) where

$$\alpha_0 = \frac{\tau^{y-1}|\cos(\pi y/2)|}{2c_0}. \tag{25}$$

Likewise, the propagation constant is computed by taking the real part of Eq. (24), yielding Eq. (10) in Ref. 23. Hence, Eq. (24) agrees with the phase velocity predicted by the Kramers–Kronig relations and the local time-causal theory.[49] Note that other FPDE models for power law media, such as the Szabo wave equation[18] and the power law FPDE in Ref. 50, satisfy the same relationship.

IV. RESULTS

This section evaluates the lumped parameter values μ, E_0, η_0, and (M,N) using published values for attenuation coefficients and other acoustic parameters. Given values of the attenuation constant α_0, the power law exponent y, the speed of sound c_0, and the density ρ_0, values for the generalized viscosity μ, an equivalent coefficient of viscosity η_0, and Young's modulus E_0 may be computed using the relations derived in Secs. II and III. In addition, given a specified power law exponent y, a recursive ladder may be constructed using Eq. (10). Measured attenuation, sound speed, and density values from Ref. 4 were utilized in these calculations. To compute the generalized viscosity μ, Eqs. (20) and (25) are combined, yielding

$$\mu = \frac{3\alpha_0 c_0^3\rho_0}{2|\cos(\pi y/2)|}. \tag{26}$$

Once μ is determined, Young's modulus E_0 and coefficient of viscosity η_0 are computed using Eq. (13) subject to the constraint $\eta_0\omega_{\max}/E_0 \ll 1$, where $\omega_{\max}=2\pi f_{\max}$ is the largest angular frequency of interest. These attenuation data are measured over a range of frequencies between 0.5 and 10 MHz, which are typical operating frequencies in diagnostic and therapeutic ultrasound. Since the fractal ladder model allows independent values for both E_0 and η_0, the coefficient of viscosity η_0 was fixed using the total viscosity of water (shear plus bulk) at room temperature[51] $\eta_0 \approx 0.004$ Pa s. This choice for η_0 satisfies the above constraint for all cases considered in this analysis.

Table I displays the results of this procedure for four tissue types: (1) breast fat, (2) liver, (3) spleen, and (4) cyst fluid. From the results of this analysis, there is a large range of predicted generalized viscosity μ values. Breast fat has the smallest generalized viscosity (3.18×10^3 Pa s), while liver has the largest generalized viscosity (2.32×10^6 Pa s). Spleen and cyst fluid have intermediate values of μ given by 8.96×10^4 and 1.30×10^4 Pa s, respectively. This large variation in μ values is attributed to the large variation in (1) the

TABLE I. Equivalent generalized viscosity μ, Young's modulus values E, and ladder parameters (M,N) calculated using density, speed of sound, and attenuation parameters from Ref. 4. The equivalent Young's modulus is calculated assuming an equivalent bulk viscosity of water $\eta_0=0.004$ Pa s.

Tissue	Breast fat	Liver	Spleen	Cyst fluid
Density ρ_0 (kg/m^3)	930	1050	1054	1000
Sound speed c_0 (m/s)	1436	1578	1567	1568
Attenuation constant α_0 (Np/cm MHz^y)	0.086	0.046	0.046	0.0058
Exponent y	1.50	1.14	1.30	1.29
Predicted generalized viscosity μ (Pa s)	3.18×10^3	2.32×10^6	8.96×10^4	1.30×10^4
Predicted Young's modulus E_0 (MPa)	500	24.1	39.7	1.89
Ladder parameters (M,N)	(0,0)	(0,2)	(1,3)	(1,4)

observed attenuation coefficient values over the frequency range 1–10 MHz and (2) the $|\cos(\pi y/2)|$ factor in the denominator of Eq. (26), which amplifies μ for y values near unity. Consequently, there is also a large range of equivalent Young's modulus values, ranging from a maximum value of 500 MPa for breast fat to a minimum value of 1.89 MPa for cyst fluid. Liver and spleen have intermediate equivalent Young's moduli of 24.1 and 39.7 MPa, respectively. Also, the low-frequency limit $\eta_0 s/E_0 \ll 1$ is satisfied for this combination of parameters. For instance, in breast fat, $\eta_0 s/E_0 \ll 1$ for frequencies less than 1 GHz, which is satisfactory for diagnostic and therapeutic applications of ultrasound. On the other hand, for cyst fluid, the low-frequency limit is only valid up to about 10 MHz.

Given a power law exponent y, approximate values of (M,N) for the recursive depth of the ladder are calculated via Eq. (10), yielding

$$y = \frac{3}{2} - \frac{1}{2^{N+1}} + \frac{1}{2^{M+1}}. \tag{27}$$

From the computed values of (M,N) in Table I, breast fat is well modeled by the simple ladder $(M,N)=(0,0)$, while liver, spleen, and cyst fluid require recursive ladder topologies. Liver is approximated by a (0,2) ladder, spleen by a (1,3) ladder, and cyst fluid by a (1,4) ladder. Since the simple ladder has an equal number of springs and dashpots, breast fat has equal elastic and viscous contributions according to the proposed model. However, liver, spleen, and cyst fluid all require greater recursive spring depths N to match the observed power law exponents. In the (0,2) ladder that approximates liver, twice as many springs are present relative to dampers. Hence, according to the recursive fractal ladder, liver has a greater contribution from the elastic, as opposed to the viscous, component. Spleen and cyst fluid, which are modeled by (1,3) and (1,4) ladders, also have more springs than dashpots in the ladder and are hence more elastic than viscous.

The ladder model demonstrates how a small coefficient of viscosity may be combined with springs that have large Young's modulus to produce an attenuation coefficient that is large relative to that of water. Furthermore, in this model, Young's modulus E_0 is more than an order of magnitude smaller in liver than in breast fat. This behavior is expected for two reasons: (1) the attenuation constant α_0 is smaller for liver than for fat and (2) the recursive ladder model for liver ($M=2$ and $N=0$, yielding $y=1.125\approx1.14$) contains about two times as many springs as fat, which is well modeled by a simple ladder ($M=N=0$) that predicts a power law exponent $y=1.5$.

V. DISCUSSION

A. Bio-mechanical interpretation

The physical significance of the power law exponent is explored in this section. The order of the fractional derivative β and hence the power law exponent y are determined by the recursion level of the damper-ladders M and spring ladders N using Eq. (10). The fractal ladder model is applicable to four special cases, each of which is discussed below.

Case I: Micro-homogeneous media ($y=2$). Let $E=0$ and $\eta>0$. The viscous theory is recovered using a single dashpot, yielding a power law coefficient of $y=2$. In this degenerate case, the model is not fractal. Due to the lack of springs, the medium is homogeneous at all scales much smaller than a wavelength, thereby indicating a lack of micro-heterogeneity.

Case II: Simple ladder model ($y=3/2$). Let $M=N=0$. This case is the simple ladder topology shown in Fig. 3. The behavior of breast fat is captured by the simple ladder model, where the contributions from the elastic and viscous components are roughly equal. The $y=3/2$ case is also recovered if $M=N$ ($\neq0$) where the relative depth of recursion of dampers and springs is the same.

Case III: Recursive ladder model with $M<N$ ($1<y<3/2$). In this case, the depth of recursion of springs is greater than the depth of recursion of dampers. Hence, at any given level of the ladder, there are more springs than dampers, indicating that the medium has a greater elastic component than viscous component. Since springs correspond to elastic structures such as cellular and nuclear membranes, while dampers correspond to inter- and intra-cellular fluids such as cytoplasm, the exponent y measures the relative mechanical contributions of elastic versus viscous structures. The power law exponent y ranges from 1 to 1.5 in this case, which is typical for most soft tissue.[4] For instance, anatomical media such as liver have y close to 1 due to the relatively complex tissue structure. This suggests that soft tissue generally has a greater elastic component than viscous component, and these elastic components play a greater role in the dissipation of ultrasonic energy.

Case IV: Recursive ladder model with $M>N$ ($3/2<y<2$). In this case, the depth of recursion of dampers is

greater than the depth of recursion of springs. Therefore, at any level of the ladder, there are more dampers than springs, indicating that the medium has a greater viscous component than elastic component. The power law y ranges from 1.5 to 2 in this case, which is typical for complex fluids like castor oil and silicone fluid.[52]

The compound ladder model also sheds light on the dependence of the power law exponent on the pathological state of tissue. For example, in Ref. 5, the power law exponent y in normal liver exhibits $y \approx 1.1$, whereas y ranges from 1.25 to 1.4 in fatty liver. The increase in the power law exponent has been explained in terms of an increase in Rayleigh scattering in fatty liver relative to healthy liver.[5] Within the context of the present compound ladder model, the increase in y is explained as an increase in the viscous microstructure relative to healthy liver, which has a greater elastic component.

The recursive ladder model provides an explanation for the combined effects of absorption and incoherent scattering in biological media. First, note that the (local) speed of sound is a function of the spring constant E by combining Eqs. (20) and (25), and the frequency-dependent phase velocity. Thus, the fractal arrangement of springs qualitatively accounts for sound speed inhomogeneity at multiple spatial scales, resulting in incoherent scattering of an incident sound field. However, sound speed inhomogeneity is not solely responsible for the observed power law dependence of the attenuation coefficient. In addition, a viscous mechanism is required to dissipate both the incident and incoherently scattered sound fields. This viscous mechanism, like the sound-speed inhomogeneity, is represented at multiple spatial scales by the fractal model. The interactions between these two mechanisms are mediated by the hierarchical arrangement of springs and dashpots. Finally, the results obtained with the fractal ladder network, which predicts an exponent y ranging between 1 and 2, agrees with the bulk of experimental data collected for soft tissues, which is effectively modeled by a power law attenuation coefficient with $1 < y \leqslant 1.5$.

B. Fractal networks

Although the present model does not correlate the underlying tissue morphology with the power law exponent, some potentially meaningful information can be extracted from the computed values. Since the current model does not consider underlying tissue morphology, the parameters (M,N) cannot be interpreted in terms of tissue complexity. For instance, breast fat has a more complicated structure that cyst fluid, yet breast fat is described by a simple ladder whereas cyst fluid requires a recursive ladder. To extend this model, more sophisticated fractal networks, such as Sierpinski gaskets, may be considered.

Beginning with the pioneering work of Mandelbrot, fractal geometry has been a useful tool to explain the self-similar structure (e.g., alveolar surfaces, cell membranes, etc.) found in biological systems.[53] More recently, fractal geometry has been applied to understanding the pathological architecture of tumors.[54] Since the vasculature of tumors is more tortuous than healthy tissue, the measured fractal dimension of tumor vessels is significantly larger than normal veins and arteries.[54] To interpret the power law exponent within the context of fractal geometry, which was discussed in Ref. 20, a quantitative relationship is provided by applying the analysis presented in Ref. 41. In Ref. 41, a constitutive equation for cross-linked polymers is derived by first assuming a fractal arrangement of springs and dashpots with spectral dimension d_s and then formulating an equivalent random walk problem. The spectral dimension d_s is related to the vibrational properties of the underlying fractal network, such as the density of normal modes in the low-frequency limit.[55,56] Intuitively, d_s measures the connectivity of a fractal network and may be tailored to different tissue types. In future work, the ladder models developed in this paper will be extended to these more general fractal networks.

C. Inhomogeneous media and nonlinear media

In general, biological medium is inhomogeneous on both the microscopic scale (~ 1 μm) and the macroscopic scale (~ 1 mm). The fractional derivative operator in Eq. (21) accounts for the effect of micro-heterogeneity on the macroscopic scale. However, Eq. (21) does not account for the macro-heterogeneity that is responsible for coherent scattering. To incorporate macro-heterogeneity, the material properties of density $\rho_0(\mathbf{r})$, adiabatic compressibility $\kappa_0(\mathbf{r})$, and shear viscosity $\mu(\mathbf{r})$ are assumed to be functions of space. By utilizing the constitutive equation in Eq. (14), an inhomogeneous 3D fractional wave equation [see Eq. (11) in Ref. 23] may be derived via the methods presented in Sec. III. In addition, the 3D fractional wave equation, as derived in Sec. III, assumes small amplitude oscillations and negligible heat conduction by utilizing a linear, adiabatic equation of state. Although the adiabatic hypothesis is justified in most biological media due to negligible thermal conductivity, the linear assumption is not justified in many biomedical applications where large amplitude effects occur.[57] However, most nonlinear models, such as Burgers equation and Westervelt's equation, assume a thermoviscous dissipation mechanism, resulting in an attenuation coefficient with frequency-squared dependence. In order to combine the effects of power law attenuation with nonlinearity, several authors have formulated nonlinear FPDEs.[18,20,24] Finite amplitude effects may be incorporated into the 3D fractional wave model by augmenting the equation of state with a quadratic term. Utilizing the stress tensor given by Eq. (14), a nonlinear generalization of the 3D fractional wave equation may be derived for both homogeneous and inhomogeneous media. The competing effects of nonlinearity and power law dissipation may then be studied within the presented framework.

VI. CONCLUSION

This paper proposes a fractal ladder network of springs and dashpots to model wave propagation in power law attenuation media. Both a simple and a recursive fractal ladder model are considered in order to capture the viscoelastic, self-similar, and hierarchical properties of biological tissue. These fractal ladders capture the hierarchical arrangement of elastic and viscous components present in biological media.

The simple fractal ladder network produces a stress-strain relationship with a fractional derivative of order 1/2, while the recursive fractal ladder produces fractional derivatives of all orders between 0 and 1. Hence, the resulting constitutive equation interpolates between a Hookean solid and Newtonian fluid via the Riemann–Liouville fractional derivative operator.

When the constitutive equation in Eq. (14) is combined with the linear equation of state and the linear equations of mass and momentum conservation, Eq. (21), which models longitudinal wave propagation in power law media via a time-fractional derivative, is derived. Hence, a fractional PDE is derived from a fractal description of the medium. The attenuation coefficient computed from this constitutive equation follows a power law in the low-frequency limit. The ladder model is compared with measured attenuation data, thereby determining an equivalent Young's modulus and the topology of the ladder model.

ACKNOWLEDGMENTS

The authors thank Mark M. Meerschaert, Department of Statistics and Probability, Michigan State University, and Stephen W. Wheatcraft, Department of Geological Sciences and Engineering, University of Nevada, Reno, for useful discussion and advice. The drawings in Fig. 1 were prepared by Amy Albin, Department of Zoology, Michigan State University. Figures 3–5 were prepared by Christopher Johnson, Department of Electrical and Computer Engineering, Michigan State University. This work was funded in part by NIH Grant No. 1R21 CA121235 J.F.K. also acknowledges support from the NRC Postdoctoral Associateship program.

APPENDIX A: RIEMANN LIOUVILLE FRACTIONAL DERIVATIVES

The Riemann–Liouville fractional derivative is formally defined via a hyper-singular integral[58]

$$\frac{d^y f}{dt^y} = \frac{1}{\Gamma(-y)} \int_{-\infty}^{t} \frac{f(t')}{(t-t')^{1+y}} dt', \tag{A1}$$

where $\Gamma(z)$ is the gamma function. By letting $y<0$ in Eq. (A1), a fractional integration is realized. The following Laplace transform relationship for fractional derivatives is necessary:

$$\mathcal{L}\left(\frac{d^y g}{dt^y}\right) = s^y \mathcal{L}(g). \tag{A2}$$

Letting $s=j\omega$ yields the Fourier transform relationship

$$\mathcal{F}\left(\frac{d^y g}{dt^y}\right) = (j\omega)^y \mathcal{F}(g). \tag{A3}$$

APPENDIX B: RECURSIVE FRACTAL LADDER MODELS

Recursive ladders are constructed in this section. Consider a ladder model constructed by replacing each of the viscous dampers in Fig. 3 with a fractal ladder, producing the arrangement shown in Fig. 4. That is, a simple ladder is embedded within a larger ladder along with springs that have elastic coefficients E, denoted by a (0,1) network, as shown in Fig. 4. Computation of $\hat{g}(s)$ for this model using the low-frequency approximation given by Eq. (7) yields $\hat{g}(s) \approx E^{3/4}\eta^{1/4}s^{1/4}$. This construction may be extended by embedding a ladder within a ladder, yielding a (0, 2) network. This recursive ladder network is further generalized to N-1 level ladders alternating with springs to create an N-level ladder-spring network, yielding $\hat{g}(s) \approx E^{1-1/2^{N+1}}\eta^{1/2^{N+1}}s^{1/2^{N+1}}$. By performing an inverse Laplace transform, fractional derivative stress-strain relationships of order 1/2, 1/4, 1/8,… are generated. As the depth of the ladder increases ($N\to\infty$), $\hat{g}(s)\to E$, yielding a purely elastic response.

A similar recursive mechanical network is constructed with dashpots and fractal ladders, as shown in Fig. 5. Evaluating the transfer function for this recursive ladder yields $\hat{g}(s) \approx E^{1/4}\eta^{3/4}s^{3/4}$. This model may also be generalized to dampers alternating with N-1 level ladders, producing $\hat{g}(s) \approx E^{1/2^{N+1}}\eta^{1-1/2^{N+1}}s^{1-1/2^{N+1}}$. By performing an inverse Laplace transform, fractional derivative stress-strain relationships of order 1/2, 3/4, 7/8,… are generated. As the depth of the ladder increases ($N\to\infty$), $\hat{g}(s)\to \eta s$, yielding a purely viscous response.

In order to generate fractional derivatives of all orders within the unit interval, fractal ladders containing alternating damper-M ladders and N ladder-spring networks are denoted as an (M,N) ladder. The (M,N) ladder is constructed by replacing the dampers in Fig. 3 with M-level damper-ladders and the springs in Fig. 3 with N-level spring ladders. Using this notation, the recursive ladder shown in Fig. 4 is denoted as (0,1), while the recursive ladder shown in Fig. 5 is denoted as (1,0). Computing the frequency-domain modulus for an (M,N) network yields

$$\hat{g}(s) \approx E^{1/2(1+(1/2^M)-(1/2^N))}\eta^{1/2(1-(1/2^M)+(1/2^N))} \times s^{1/2(1-(1/2^M)+(1/2^N))}. \tag{B1}$$

Letting $\beta=1/2(1-1/2^M+1/2^N)$ and performing an inverse Laplace transform yields Eq. (9).

[1] S. A. Goss, L. A. Frizzell, and F. Dunn, "Ultrasonic absorption and attenuation in mammalian tissues," Ultrasound Med. Biol. **5**, 181–186 (1979).
[2] F. T. D'Astous and F. S. Foster, "Frequency dependence of ultrasound attenuation and backscatter in breast tissue," Ultrasound Med. Biol. **12**, 795–808 (1986).
[3] P. He, "Experimental verification of models for determining dispersion from attenuation," IEEE Trans. Ultrason. Ferroelectr. Freq. Control **46**, 706–714 (1999).
[4] F. A. Duck, *Physical Properties of Tissue*, 1st ed. (Academic, London, 1990), pp. 99–124.
[5] P. A. Narayana and J. Ophir, "On the frequency dependence of attenuation in normal and fatty liver," IEEE Trans. Sonics Ultrason. **SU-30**, 379–383 (1983).
[6] T. Lin, J. Ophir, and G. Potter, "Frequency-dependent ultrasonic differentiation of normal and diffusely diseased liver," J. Acoust. Soc. Am. **82**, 1131–1138 (1987).
[7] P. M. Morse and K. U. Ingard, *Theoretical Acoustics* (Princeton University Pres, Princeton, NJ, 1968), pp. 270–300.
[8] M. A. Biot, "Theory of propagation of elastic waves in fluid-saturated porous solid. I. Low-frequency range," J. Acoust. Soc. Am. **28**, 168–178 (1956).
[9] A. I. Nachman, J. F. Smith, and R. C. Waag, "An equation for acoustic propagation in inhomogeneous media with relaxation losses," J. Acoust. Soc. Am. **88**, 1584–1595 (1990).

[10]A. C. Kak and K. A. Dines, "Signal-processing of broad-band pulsed ultrasound—Measurement of attenuation of soft biological tissues," IEEE Trans. Biomed. Eng. **25**, 321–344 (1978).
[11]K. V. Gurumurthy and R. M. Arthur, "A dispersive model for the propagation of ultrasound in soft tissue," Ultrason. Imaging **4**, 355–377 (1982).
[12]T. L. Szabo, "The material impulse response for broadband pulses in lossy media," in Proceedings of the IEEE Ultrasonics Symposium, Honolulu, HI (2003), pp. 748–751.
[13]P. He, "Simulation of ultrasound pulse propagation in lossy media obeying a frequency power law," IEEE Trans. Ultrason. Ferroelectr. Freq. Control **45**, 114–125 (1998).
[14]M. G. Wismer and R. Ludwig, "An explicit numerical time domain formulation to simulate pulsed pressure waves in viscous fluids exhibiting arbitrary frequency power law attenuation," IEEE Trans. Ultrason. Ferroelectr. Freq. Control **42**, 1040–1049 (1995).
[15]R. S. C. Cobbold, N. V. Sushilov, and A. C. Weathermon, "Transient propagation in media with classical or power-law loss," J. Acoust. Soc. Am. **116**, 3294–3303 (2004).
[16]S. Leeman, "Ultrasound pulse propagation in dispersive media," Ultrasound Med. Biol. **25**, 481–488 (1980).
[17]J. M. Blackledge and S. Leeman, "Green's functions for acoustic fields in dispersive media," J. Phys. D: Appl. Phys. **16**, L247–L250 (1983).
[18]T. L. Szabo, "Time-domain wave-equations for lossy media obeying a frequency power-law," J. Acoust. Soc. Am. **96**, 491–500 (1994).
[19]A. Hanyga and M. Seredyńska, "Power-law attenuation in acoustic and isotropic anelastic media," Geophys. J. Int. **155**, 830–838 (2003).
[20]W. Chen and S. Holm, "Fractional Laplacian time-space models for linear and nonlinear lossy media exhibiting arbitrary frequency power-law dependency," J. Acoust. Soc. Am. **115**, 1424–1430 (2004).
[21]R. Schumer, D. A. Benson, M. M. Meerschaert, and S. W. Wheatcraft, "Eulerian derivation of the fractional advection-dispersion equation," J. Contam. Hydrol. **48**, 69–88 (2001).
[22]M. Caputo, "Linear models of dissipation whose *Q* is almost frequency independent II," Geophys. J. R. Astron. Soc. **13**, 529–539 (1967).
[23]M. G. Wismer, "Finite element analysis of broadband acoustic pulses through inhomogeneous media with power law attenuation," J. Acoust. Soc. Am. **120**, 3493–3502 (2006).
[24]M. Ochmann and S. Makarov, "Representation of the absorption of nonlinear waves by fractional derivatives," J. Acoust. Soc. Am. **94**, 3392–3399 (1993).
[25]Z. E. A. Fellah and C. Depollier, "Transient acoustic wave propagation in rigid porous media: A time-domain approach," J. Acoust. Soc. Am. **107**, 683–688 (2000).
[26]T. L. Szabo and J. Wu, "A model for longitudinal and shear wave propagation in viscoelastic media," J. Acoust. Soc. Am. **107**, 2437–2446 (2000).
[27]M. Giona and H. E. Roman, "Fractional diffusion equation on fractals: One-dimensional case and asymptotic behavior," J. Phys. A **25**, 2093–2105 (1992).
[28]R. Metzler, W. G. Glöckle, and T. F. Nonnenmacher, "Fractional model equation for anomalous diffusion," Physica A **211**, 13–24 (1994).
[29]W. G. Glöckle and T. F. Nonnenmacher, "Fox function representation of non-Debye relaxation processes," J. Stat. Phys. **71**, 741–756 (1993).
[30]H. Schiessel, R. Metzler, A. Blumen, and T. F. Nonnenmacher, "Generalized viscoelastic models: Their fractional equations with solutions," J. Phys. A **28**, 6567–6584 (1995).
[31]R. L. Bagley and P. J. Torvik, "A theoretical basis for the application of fractional calculus to viscoelasticity," J. Rheol. **27**, 201–210 (1983).
[32]J. Wu and C. Layman, "Wave equations, dispersion relations, and van Hove singularities for applications of doublet mechanics to ultrasound propagation in bio- and nanomaterials," J. Acoust. Soc. Am. **115**, 893–900 (2004).
[33]N. W. Tschoegl, *The Phenomenological Theory of Linear Viscoelastic Behavior: An Introduction* (Springer-Verlag, Berlin, 1989).
[34]C. T. Lim, E. H. Zhou, and S. T. Quek, "Mechanical models for living cells A review," J. Biomech. **39**, 195–216 (2006).
[35]A. Yeung and E. Evans, "Cortical shell-liquid core model for passive flow of liquid-like spherical cells into micropipets," Biophys. J. **56**, 139–149 (1989).
[36]E. M. Darling, M. Topel, S. Zauscher, T. P. Vail, and F. Guilak, "Viscoelastic properties of human mesenchymally-derived stem cells and primary osteoblasts, chondrocytes, and adipocytes," J. Biomech. **41**, 454–464 (2008).
[37]J. D. Humphrey, "Continuum biomechanics of soft biological tissues," Proc. R. Soc. London, Ser. A **459**, 3–46 (2003).
[38]C. Verdier, "Rheological properties of living materials. From cells to tissues," J. Theoretical Medicine **5**, 67–91 (2003).
[39]B. Gross and R. M. Fuoss, "Ladder structures for representation of viscoelastic systems," J. Polym. Sci. **19**, 39–50 (1956).
[40]H. Schiessel and A. Blumen, "Hierarchical analogues to fractional relaxation equations," J. Phys. A **26**, 5057–5069 (1993).
[41]H. Schiessel and A. Blumen, "Mesoscopic pictures of the sol-gel transition: Ladder models and fractal networks," Macromolecules **28**, 4013–4019 (1995).
[42]N. Heymans and J.-C. Bauwens, "Fractal rheological models and fractional differential equations for viscoelastic behavior," Rheol. Acta **33**, 210–219 (1994).
[43]B. Alberts, A. Johnson, J. Lewis, M. Raff, K. Roberts, and P. Walter, *Molecular Biology of the Cell*, 4th ed. (Garland Science, New York, 2002).
[44]B. Gross, "Ladder structures for representation of viscoelastic systems. II," J. Polym. Sci. **20**, 123–131 (1956).
[45]R. C. Koeller, "Applications of fractional calculus to the theory of viscoelasticity," J. Appl. Mech. **51**, 299–307 (1984).
[46]P. E. Rouse, "A theory of linear viscoelastic properties of dilute solutions of coiling polymers," J. Chem. Phys. **21**, 1272–1280 (1953).
[47]A. Kreis and A. C. Pipkin, "Viscoelastic pulse propagation and stable probability distributions," Q. Appl. Math. **44**, 353–360 (1986).
[48]M. J. Buckingham, "Causality, Stokes' wave equation, and acoustic pulse propagation in a viscous fluid," Phys. Rev. E **72**, 026610 (2005).
[49]T. L. Szabo, "Causal theories and data for acoustic attenuation obeying a frequency power-law," J. Acoust. Soc. Am. **97**, 14–24 (1995).
[50]J. F. Kelly, M. M. Meerschaert, and R. J. McGough, "Analytical time-domain Green's functions for power-law media," J. Acoust. Soc. Am. **124**, 2861–2872 (2008).
[51]L. E. Kinsler, A. R. Frey, A. B. Coppens, and J. V. Sanders, *Fundamentals of Acoustics*, 4th ed. (Wiley, New York, 2000), pp. 210–245.
[52]K. R. Waters, M. S. Hughes, J. Mobley, G. H. Brandenburger, and J. G. Miller, "On the applicability of Kramers-Krönig relations for ultrasonic attenuation obeying a frequency power law," J. Acoust. Soc. Am. **108**, 556–563 (2000).
[53]E. R. Weibel, "Fractal geometry: A design principle for living organisms," Am. J. Physiol. Lung Cell. Mol. Physiol. **261**, L361–L369 (1991).
[54]J. W. Baish and R. K. Jain, "Fractals and cancer," Cancer Res. **60**, 3683–3688 (2000).
[55]D. Dhar, "Lattices of effectively nonintegral dimensionality," J. Math. Phys. **18**, 577–585 (1977).
[56]S. Alexander and R. Orbach, "Density of states on fractals: Fractons," J. Phys. (Paris) **43**, L625–L631 (1982).
[57]G. Wojcik, J. Mould, F. Lizzi, N. Abboud, M. Ostromogilsky, and D. Vaughn, "Nonlinear modeling of therapeutic ultrasound," in Proceedings of the IEEE Ultrasonics Symposium, Cannes, France (1995), pp. 1617–1622.
[58]A. A. Kilbas, H. M. Srivastava, and J. J. Truhillo, *Theory and Applications of Fractional Differential Equations* (Elsevier, Amsterdam, 2006).